Author version: Energy 215 (2021) 119122

Methodological analysis of variable geometry turbine technology impact on the performance of highly downsized Spark-Ignition engines

José Ramón Serrano[1], Pedro Piqueras[1], Joaquín De la Morena*[1], Alejandro Gómez-Vilanova[1], Stéphane Guilain[2]

[1] CMT-Motores Térmicos, Universitat Politècnica de València, Valencia 46022, Spain

[2] Renault Nissan Mitsubishi, 1 Allée Cornuel Lardy 91510, France

* Corresponding author: joadela@mot.upv.es

Keywords: turbocharger, engine, modeling, torque, fuel consumption

ABSTRACT

New generation of spark ignition (SI) engines are expected to represent most of the future market share in a context of powertrain hybridization. Nevertheless, the current technology has still critical challenges in front to meet incoming CO2 and pollutant emissions standards, so new technologies are emerging to improve engine efficiency. In parallel to combustion concepts, a key required trend is downsizing based on high engine boosting. New turbocharger technologies, such as variable geometry turbines (VGT), become suitable for its application under the demanding operating conditions of SI engines. In this work, a methodology for the analysis of the VGT usage in comparison with traditional waste-gate (WG) turbine is presented. From experimental data obtained in engine test cell, a theoretical analysis aimed at ensuring full control on turbine boundary conditions, such as combustion variability, compressor map or engine calibration, was conducted. Taking advantage of

highly validated and physically representative 1-D gas-dynamics and turbocharger models, the engine performance is discussed as a function of the turbine technology at full and partial load in a wide range of engine speed at the same time as the altitude impact is addressed. In all, it was found that VGT technology shows less limitations in extreme working conditions, such as low- and high-end torque regions, where the WG technology represents a limitation in terms of the maximum power output. Full load differences become more even more evident in altitude working conditions. When it comes to partial loads, differences in fuel consumption are minor, but potentially beneficial for VGTs.

NOMENCLATURE

BEV	Battery Electric Vehicle
BSFC	Brake Specific Fuel Consumption
CA50	Crank angle for 50% heat release
CNN	Combustion Neural Network
EIVC	Early intake valve closure
FL	Full load
GHG	Green House Gasses
HTM	Heat transfer multiplier
ICE	Internal Combustion Engine
p	Pressure
PL	Partial load
pmep	Pumping Mean Effective Pressure
SI	Spark Ignition
T	Temperature
TOC	Time of Combustion
VGT	Variable Geometry Turbine

WG	Waste Gate
1-D	One dimensional
2	Compressor outlet stage
2’	Engine intake manifold stage
3	Turbine inlet stage
4	Turbine outlet stage

1. INTRODUCTION

After the diesel-gate event, diesel engines for automotive purposes, are falling into disuse as they become unpopular, as Gross & Sonnberger stated in [1]. In this context, worldwide market requirements are to be covered by another technology: the hybridized spark ignition (SI) turbocharged engines [2].

However, fuel consumption is still the main disadvantage of SI engines in comparison to diesel ones. An overview of CO2 reduction technologies applied to gasoline engines as a response to greenhouse gases (GHG) standards and customer demand for fuel efficiency draws a complex scenario [3]. With the purpose of reaching the high efficiency of compression ignition engines, SI engines studies dealing with valve timing control strategies [4] or thermal management [5] arise. Complementary, hybridization becomes one of the main selected strategies by engine developers in modern SI engines. As discussed by Geng et al. [6], the hybrid powertrains may contribute in a high degree to enhance the fuel economy and reduce the pollutant emissions. What is more, the electric power unit may back the ICE during sudden maneuvers. Recent studies have also shown that there are synergies between advanced technologies in SI engine (such as variable valve actuation and variable compression ratio) and hybrid powertrain architectures to provide further benefits in fuel consumption [7].

The life cycle assessment points out that GHG emissions attributed to internal combustion engines (ICEs) are around 50% higher than in the case of battery electric vehicles (BEV) [8]. However, the extensive use of BEVs involves relevant drawbacks concerning rare earth materials elements gathering, manufacturing emissions and batteries availability [9]. A BEV of approximately 400 km range, requires a 60 kWh battery, weighting around 500kg. The investment corresponds to approximately forty 1.5kWh batteries for full hybrid vehicles (FHV). In all, FHV may gather the benefits of both technologies, while minimizing the drawbacks: materials collecting and batteries disposal issues are minimized, the SI engine operating range is reduced to higher fuel economy working areas. In addition batteries may also charge themselves during braking maneuvers [10] and drive the vehicle under very low power demand, where the brake specific fuel consumption (BSFC) of SI engine is much worse.

In addition, thanks to downsizing, in parallel to down-speeding the reduction of mechanical and heat losses is guaranteed, thus contributing to reduce further the BSFC and, hence, the CO2 emissions [11]. A smaller engine architecture implies higher engine boosting if the performance is attempted to be kept. Consequently, the turbocharger operation and its interaction with the rest of the engine hardware become more relevant for engine efficiency [12]. New turbocharger technologies in the context of series SI engines become potential technical solutions when improving nowadays' fuel consumption and power figures. Asymmetric twin-scroll turbocharging [13], self-recirculating case treatment [14] and combinations of variable geometry and twin scroll [15] are some examples new turbocharger technologies improvements for ICE.

In this context, researchers have developed different numerical approaches over the last years to fully understand the implications of turbine operation on the engine. Serrano et al. used 3D-CFD tools to analyze tip losses at extreme blade-speed ratio conditions [16], and then used these learnings to develop a methodology for extrapolating turbine maps

needed for engine 1D simulations [17]. Ding et al. [18] employed a turbine 1D model for evaluating its performance at pulsating conditions such as those occurring in ICE. Bozza et al. [19] also explored exhaust gas recirculation as a means to overcome turbine inlet temperature limitations through 1D engine modeling. Sandoval et al. [20] developed a methodology to characterize turbocharger performance on driving conditions.

In the current study, variable geometry turbines (VGT), are compared to the SI ICE standard turbine: the waste-gate (WG). In WG turbines, part of the exhaust gas flow by-passes a fixed turbine geometry. Therefore, the amount of by-passed flow becomes the boost-level controlling parameter. By-passing the turbine as boost-pressure control strategy, partially wastes the available exhaust gas flow enthalpy, damaging the turbine efficiency. By contrast, VGTs modify the vanes passage geometry to fulfill the boost demand. Since all the exhaust mass flow is expanded, VGTs provide higher efficiency and result in a better matching throughout a wider operative range [21]. Nevertheless, this kind of turbine technology can suffer from deformation and eventual stack of the mechanism when exposed at high temperature. For this reason, it has been widely used for compression-ignition engines, where the maximum turbine inlet temperature is in the range of 850-870ºC. Instead, stoichiometric operation in SI engines leads to higher values (up to 1000ºC), limiting the implementation of this technology since extreme levels of fuel enrichment would be needed. However, material technology improvements (partially motivated by SI engines requirements) have allowed the availability of the first VGT prototypes for SI application in the past few years.

The lack of hardware availability targeted for SI engines has also limited the amount of studies in the literature about this topic. Sjeric et al. [22] used engine 1D simulations to evaluate the potential of VGT coupled with exhaust gas recirculation for fuel consumption improvements on SI engines. Andersen et al [23] evaluated six different samples of VGT, confirming performance advantages for most of them compared to a fixed geometry

turbocharger, especially at low speeds. Shimizu et al [24] pointed out that the fuel enrichment needed to be implemented to protect the VNT mechanism induced a severe increase of HC and CO emissions. Noga [25] applied VGT technology to an over-expanded engine, thanks to the higher temperature reduction, demonstrating potential to significantly increase wide open throttle performance. Tang et al. [26] evaluated the performance of such turbochargers in transient operation, highlighting the challenges of achieving a proper compromise between turbocharger acceleration and an engine volumetric efficiency loss due to excessive turbine inlet pressure. Ericsson et al. [27] studied the interaction between VGT and variable valve actuation to optimize the transient response. Wang et al. [28] studied the potential benefits of VGT combined with early intake valve closure (EIVC) to reduce knocking tendency and fuel enrichment.

The present study deals with a new generation SI 1.3L engine, as described in [29]. The complexity of a direct turbine technology comparison with merely experimental data is discussed. The test boundary conditions, the ECU calibration and the compressor side of each turbocharger become out-of-control influencing parameters. This means that purely experimental data it is not suitable for solely turbine technologies comparison.

In order to obtain a comparison between turbine technologies with the minimum possible bias, it was decided to make use of a 1-D complete engine model previously developed in [29] on GT-Suite platform. In this model, the components of the intake and exhaust paths are discretized in small elements where compressible fluid-dynamics equations are solved. Additionally, specific zero-dimensional models for some key engine elements, such as the cylinders, the compressor and the turbine, are included. Once calibrated, the engine model allows to predict the flow characteristics in the air management system on a crank-angle basis, as well as its impact on engine performance parameters such as the brake torque, the fuel consumption or the transient response.

Hence, the experimental campaign is taken as the basis for the calibration of the engine model and for the development of a combustion neural network in this study. Having reached this point, a specific modelling campaign for turbine technologies comparison is performed, overcoming experimental uncertainties. As explained by Serrano et al. [29], more realistic and accurate results are expected from the use of adiabatic turbocharger maps, as the ones used in this study. The process to obtain the aforementioned adiabatic turbocharger maps it is described in [30]. A set of full and partial load simulations are performed. In these simulations, the same engine boundaries, defined by altitude and engine speed at full-load, and compressor map for all turbines are kept. With this approach, a clear comparison between the VGT and WG technologies is provided.

Table 1 highlights the main differences between the current study and those previously performed in the literature. On the one hand, the current study is the only one providing experimental data to compare VGT and WG technologies in state of the art hardware, including direct injection, variable valve actuation and maximum temperature of 950ºC. On the other hand, it is also the only including both partial load conditions as well as altitude operation, both of them critical for the engine operation during certification cycles.

Table 1. Comparison of hardware and operating conditions between current and previous studies

Reference	**Engine**	**Turbocharger**	**Operating conditions**
Sjeric et al. [22]	1.4 liters Indirect injection Cooled HP-EGR	VGT w/ WG	Full-load (2000-5000 rpm), Fuel enrichment (λ>0.8) Simulation only
Andersen et al [23]	2.0 liters Indirect injection	6 VGTs 1 WG	Full-load (1000-6000 rpm), Max. T3=900ºC Tip-in (1250-1750 rpm) with step actuation

			Cold start
Shimizu et al [24]	0.6 liters Indirect injection 3 camshafts with different overlap	VGT w/ WG	Full-load (3000-10000 rpm), Fuel enrichment (λ>0.8)
Noga [25]	2.0 liters Direct injection 2 fired cylinders, + 2 for additional expansion	1 VGT 1 WG	Full-load (2000-3200 rpm), Stoichiometric
Tang et al. [26]	2.0 liters Direct injection Variable valve timing	1 VGT	Tip-in (1500 & 2000 rpm) with control optimization
Ericsson et al. [27]	2.0 liters Direct injection Variable valve timing	1 VGT	Tip-in (1750 rpm) Simulation only
Wang et al. [28]	1.6 liters Direct injection EIVC	1 VGT 1 WG	Full-load (1000-5000 rpm), Max. T3=950ºC Simulation only
Current study	1.4 liters Direct injection Variable valve timing	2 VGTs 1 WG	Full-load (1250-5000 rpm), Max. T3=950ºC Partial-load () Cold start

2. EXPERIMENTAL CAMPAIGN

The complete experimental campaign was developed in CMT-Motores Térmicos Research Institute laboratories. The engine unit in this study corresponds to 1.3 liters, 4-cylinder, direct injection, turbocharged SI ICE. The engine is equipped with variable valve timing (VVT) and a water charge-air cooler.

Three turbocharger units were tested: two VGTs and one WG turbine. All of them were designed following a very similar matching criterion. The experimental campaign includes information about full and partial load working points. Figure 1_A shows in different colors, the engine delivered torque for each engine-turbocharger combination. Figure 1_A also shows in black diamonds the partial load working points. No torque differences in the partial loads take place since a specified torque value was the target in the partial loads experimental campaign.

Full load campaign includes nine working points covering a speed range from 1250 to 5000 engine rpm. For all three turbocharger units, the testing strategy was the same: increasing the boost pressure (closing VGT or WG mechanism) as much as possible until a given engine or turbocharger thermo-mechanical limit was reached. The target in full load operation was to obtain the maximum possible engine break torque for each point and turbocharger. The main limits considered on that regard were: turbocharger speed, exhaust manifold pressure (p3) and temperature (T3), and compressor outlet pressure (p2) and temperature (T2). In this sense, the turbocharger speed limit has been set individually for each turbocharger sample with a 10% margin of the maximum feasible. Exhaust manifold limits (p3 and T3) have been set to 3.2 bar and 950ºC for all turbochargers. Finally, maximum compressor outlet conditions (p2=2.55 bar and T2=170ºC) are limited to ensure the durability of the plastic components in the compressor outlet piping.

While WG actuation was done through the engine control unit (ECU), the VGT position was controlled externally using a PXI™ system from National Instruments. In

parallel, the spark advance was optimized while keeping knock under control applying a knock detection and combustion diagnosis software [31] based on in-cylinder pressure measurements performed with an instrumented spark plug (AVL ZI33). The last remarkable aspect is that the air-to-fuel ratio was governed by the ECU.

Figure 1_A torque differences in full load are expected not only because of the turbocharger unit but also the impact of some out-of-control parameters variability, mainly related to ambient conditions. In full loads, the ECU enriched the fresh mixture in order to control T3 limit.

In the case of the partial load operation, the engine was controlled at a constant torque, so these variabilities are absorbed by a different throttle position, while the turbocharger actuation was fully open for all three turbocharger units. Air-to-fuel mixture was kept at stoichiometric conditions (lambda 1) in these operative points.

The usage of partial loads coupled to full loads during the calibration procedure does not only add more information, but also provide the model with a wider working range, leading to a more robust and global 1-D model.

The collected experimental information was used for the virtual engine model calibration according to the methodology described in [29]. This included the validation of the engine model as well as the adiabatized turbocharger maps. Indeed, the study shows the high importance of using adiabatic turbocharger maps. The methodology to obtain the these maps is depicted in [30].

The previously described set of experimental and model information is not suitable for a direct fair comparison of the technologies. The main reasons are:

- As previously stated, some of the boundary conditions are affected by daily and seasonal natural variations. If by chance one turbocharger is measured in winter and other in summer, T2 limitation may become more easily reachable for the one measured in summer, resulting in a potentially lower performance. Also, higher

ambient temperature may lead to higher intake manifold temperature since the WCAC is fed with coolant at room temperature. Hence, at the same volumetric efficiency the air mass flow would be reduced, and consequently the torque. Figure 1_B shows how the intake manifold temperature for VGT_1 reaches values of 55ºC due to the combination of higher T2 and higher WCAC coolant temperature, while the other two units hardly reach 35ºC.

- Secondly, as previously mentioned, the ECU governs the richness of the mixture. Mixture enrichment is a strategy for T3 limitation. However, the ECU was calibrated for the WG turbine unit. As it can be observed in Figure 1_C, T3 values for VGT's are still far from the maximum allowed temperature. These differences are mainly attributed to the extra enrichment induced by the ECU in the VGTs' test (see lambda values in Figure 1_D).
- Thirdly, the compressor coupled to each of the turbocharger units is not the same. This may hide or increase differences exclusively due to turbine technology. The different compressor map may induce variations not only in the mass flow vs. rotational speed but also in terms of compressor efficiency and surge limit.

In summary, the experimental campaign is necessary for a proper engine and turbocharger model calibration and validation but not suitable for a fair turbine technology comparison by itself. For this purpose, it is still necessary to perform calculations in which the only difference lies in the turbine, not in the boundaries or ECU calibration, neither in compressor map performance.

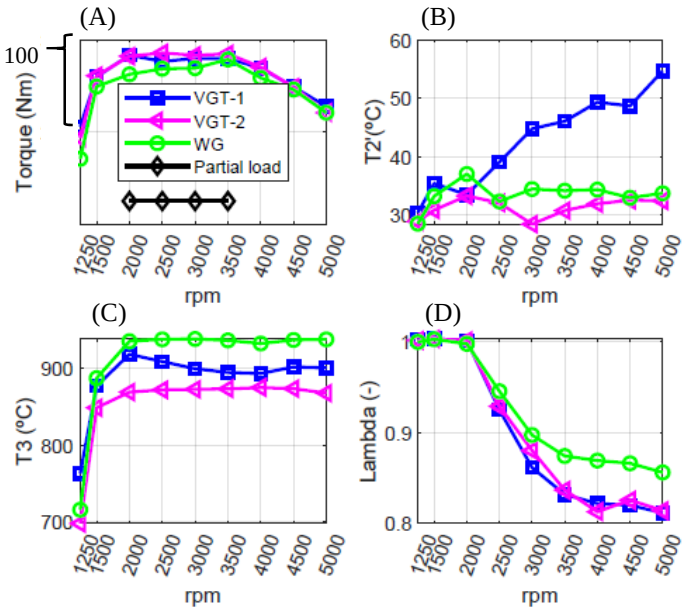

Figure 1: Experimental toque and working influencing variable

3. MODELLING CAMPAIGN

As previously stated, Serrano et al. [29] proposed a methodology to setup a complete 1-D engine model. This procedure is based in a simultaneous but independent fitting for each engine stage or element to adjust the model to the experimental campaign.

First, the turbine is decoupled from the compressor side. This way it is possible to guarantee independently the experimental p2 (through compressor speed) and p3 (through turbine VGT/WG position). In other words, the energy loop that results in each p3 for a targeted p2, through the turbocharger modelling, is by-passed during the fitting procedure. Hence, any possible uncertainty in the turbocharger maps is overcome at this stage.

Afterwards, several PIDs adjust the selected calibration parameters during the simulation. The overall cylinder heat transfer multiplier (OCHTM) adjusts the engine volumetric efficiency. Instead, the heat transfer multiplier in the water-charge air cooler (WCAC_HTM) is controlled so that the intake manifold temperature (T2') is well-reproduced by the model. The same is applied to the heat transfer multiplier in the exhaust high pressure line (E_HP_HTM), in order to target the experimental exhaust manifold temperature (T3) for

the complete engine range. The discharge coefficient in the low-pressure path of the exhaust line is directly related to the backpressure towards the turbine (p4). Finally, the heat transfer multiplier in the turbine volute allows for a fine-tuning of the heat transfer for a better turbine outlet temperature (T4) estimation. In summary, the considered parameters for the model calibration are the ones gathered in Table 2.

Table 2. Summary of fitting parameters during the model calibration procedure.

Fitting parameter	Fitted value
OCHTM	Volumetric efficiency
WCAC_HTM	T2’
E_HP_HTM	T3
E_LP_FDC	p4
V_HTM	T4

Finally, the values obtained for the complete set of fitted parameters are imposed, and turbine and compressor re-coupled. Afterwards, the calculations are run once again for the final validation. At this point, the quality of the turbochargers maps is called into question: since the model was fitted to the experimental campaign, if after the turbocharger re-coupling, simulations do not agree the experiments, it is a symptom of a wrong turbocharger maps.

The validation of the model is shown in Figure 2 and Figure 3 for full and partial loads, respectively. Dotted lines in Figure 2 represent ±3% discrepancy between model and experiments. Simulations in Figure 2 corresponds to the full load operating with VGT_1, VGT_2 and WG turbine. The accuracy in air mass flow and torque predictions (Figure 2_A and Figure 2_B respectively) show how volumetric efficiency, mechanical losses and block heat losses are well predicted. Turbine inlet and outlet temperature (T3 and T4 respectively) are shown in Figure 2_C. T3 and T4 predictions confirm the accurate heat transfer computation at the exhaust runners, manifold and turbine. Finally, p3 and p4 are shown in Figure 2_C. Turbine outlet pressure (p4) mostly depends on the air mass flow and the discharge coefficient of the exhaust line. However, p3 accuracy allows to validate turbine

maps: since T3 and p4 are well-predicted, p3 estimation becomes an indicator of turbine maps quality in terms of efficiency.

Figure 3 presents the partial load results for validation purposes. Air mass flow (Figure 3_A) and BSFC (Figure 3_B) were selected as the more representative variables for the model validation. Air mass flow is within the 3% discrepancy range. BSFC green points, corresponding to the WG, are at the edge of this 3% limit, while a more accurate prediction is reached for the other turbochargers.

In order to perform the turbines comparison, the compressor from VGT_1 was selected. In other words, from now in advance, in any calculation, the corresponding compressor sides of VGT_2 and WG units, are replaced by the one belonging to VGT_1. In addition, a common strategy for lambda control was used aimed at varying the enrichment if the turbine inlet temperature limitation is reached. The main drawback of this procedure is related to the combustion prediction. The selected way to proceed was to develop a combustion neural network (CNN). This is another stage of the model development where the availability of a wide set of experimental data plays a crucial role due to the need of neural network training. Hence, for the neural network training, a validated model is compulsory at the starting point. The steps to follow are:

1. Performing a three pressure analysis [32] for as many points as possible. For this purpose, the experimental campaign working points are simulated. The experimental instantaneous in-cylinder pressure is required as the target to be reproduced by the model. This is achieved by iteratively varying the parameters of a Wiebe's combustion law until the modeled instantaneous cylinder pressure fits (as much as possible) the experimental provided profiles. As a result, the Wiebe function parameters for combustion modelling are obtained: CA50, time of combustion (TOC) and n-parameter, which is related to the heat release shape.

2. Gathering the engine variables influencing the combustion evolution. This information is taken from the simulations corresponding to the experimental points. The variables considered are the engine speed and cylinder properties at the intake valve closing: pressure, residuals, temperature, lambda, and trapped mass.
3. Neural Network Training. Two sets of data are required for this purpose: Wiebe's combustion law parameters and combustion influencing variables. The CNN is trained in such a way that depending on the simulation combustion influencing variables combustion parameters are predicted (CA50, TOC and n-parameter).

Previous works by Galindo et al. [33] and Serrano et al. [34] provided further details about the CNN development and validation. From this point in advance, full and partial load simulations deal with the same calibrated and validated virtual engine model, including the Trained CNN for combustion prediction.

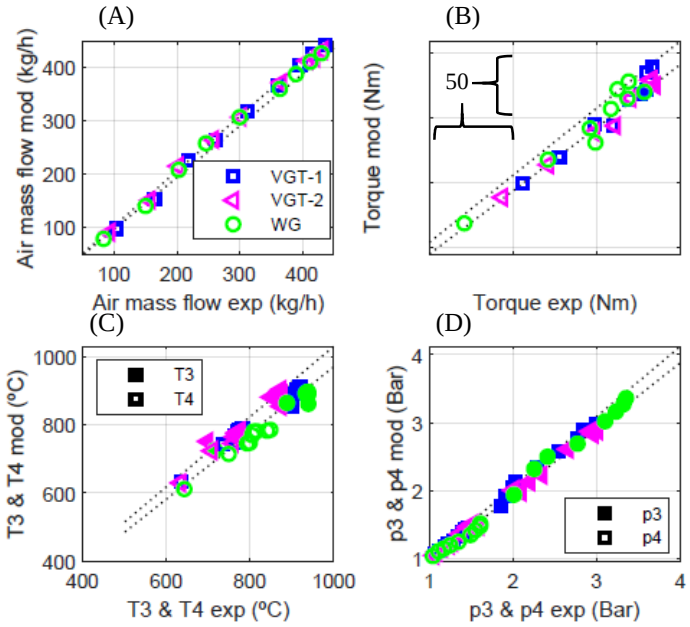

Figure 2: Full load model validation for some engine variables

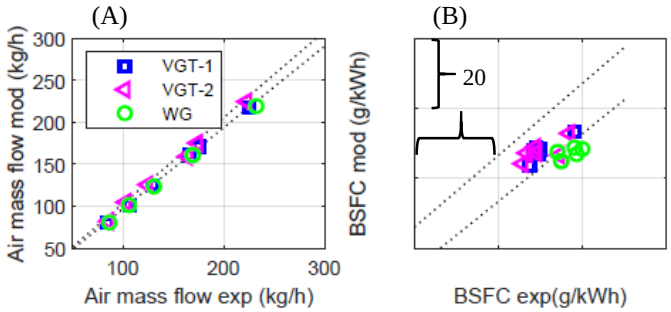

Figure 3: Partial load model validation for some engine variables

3.1 Full load results (sea level)

Figure 4 shows the full-load results for the main engine variables. Each engine or turbocharger limit is shown as a horizontal red line on the corresponding chart.

The first remarkable fact in Figure 4_A is the higher mass flow in the high-end (4000-5000 rpm) for both VGTs. The same can be said for the low-end torque (1250-1500): VGTs provide 6.9% and 12.7% higher mass flow (scale effects makes hard to appreciate the differences). The higher air mass flow goes in hand with higher torque as shown in Figure 4_B. Figure 4_C shows the torque differences in relative terms, taking WG as the reference, as in equation (1) it is specified. Figure 4_C shows how torque differences at high speed overcome the barrier of the 5%, while in the low end-torque differences go between 5% and 12.7 %.

$$Technology\ difference = \frac{VGT_{0m} - WG_{0m}}{WG_{0m}} * 100 \qquad (1)$$

The main reason for the previously presented air mass flow and torque differences in the low and high-end torque is the higher boost pressure level for VGTs (see Figure 4_D). The reason why this happens is presented as follows:

- Taking a look into the high-end torque, for both technologies, p3 limit is almost reached (see Figure 4_E). However, even if both technologies reach the maximum allowed p3,

higher p2 is achieved with the VGT. In other words, WG lower efficiency values in the high-end torque imply a p3 limitation that constrains p2 more than in the case of VGTs. This is confirmed by taking a look at turbine efficiency in Figure 4_F. Two turbine efficiencies for the WG series are shown. The dotted line corresponds to the efficiency with which the useful gas is expanded, the continuous series appeals to the actual turbine efficiency, which computes as zero the efficiency of the waste-gated gas. The predicted turbine efficiency claims higher values for both VGTs, which goes in hand with the higher boost pressure in the high-end torque. Compressor efficiency (Figure 4_G) differences are purely originated by the higher turbocharger speed (Figure 4_H) achieved with VGTs.

- In the low-end torque (1250-1500 rpm), the WG orifice is completely closed (see Figure 4_I). In other words, the turbine is too big for the operative air mass flow range corresponding to the low-end. This is the main reason why boost pressure is limited for the WG. Particularly for the VGT_1 the main limitation is related to compressor surge at 1500 rpm, while at 1250 rpm the main constraint is the turbine efficiency. If more closure is intended, efficiency loss leads to a turbocharger deceleration and p2 loss consequently. Hence, VGT_1 closure had to be artificially limited. VGT_2 performs better at every working point. In the low-end torque compressor surge is the limitation at any point.
- In the middle engine speed range (2000-3500rpm), air and torque differences are still present (see Figure 4_A and Figure 4_B). Differences are around 2% in torque in favor to VGTs. Higher torque in the VGTs is due to the systematically lower p3 requirement to reach the target p2. This is again purely attributed to higher VGTs efficiency. In any case, p3 is not a limitation (see Figure 4_E), hence the maximum p2 is always achieved by all three turbochargers. However, the difference in p3 leads to some penalty in terms of the mass flow and torque.

The aforementioned conclusions go in hand with the ones found in previous studies. Tang et al. [35] already observed the over-sized effect of fixed geometry turbines for the low-end torque, as well as the under-sized effect in the high-speed range were identified. However, the differences reported in the work by Tang et al. [35] are more noticeable than in the current study for the complete engine range. In their study, VGT showed benefits from 5 to 22 percent in the low-end torque, and 5 to 11 percent in the high-end, with respect to the WG. Instead, the current work showed maximum benefits of 11 and 8 percent, respectively.

Having analyzed the difference in performance and the reasons leading to the aforementioned differences, Figure 5 shows the results of some other engine variables that are affected by the turbine technology. First of all, Figure 5_A validates the model PID that controls T3: in the high-end torque, where T3 limitation is an issue, it is confirmed that mixture enrichment regulation does not benefit one turbocharger or another. As it can be seen in Figure 5_B, more enrichment is required for the VGTs: the higher amount of fresh air results in higher T3, consequently some extra enrichment is required for VGTs. Figure 5_C shows BSFC differences according to equation (1). Higher mixture enrichment values for VGTs are the main reason for differences in Figure 5_C. In all, high-end torque BSFC differences reach values of 7% to 11% in favor to the WG turbine.

It is worth of mention how CNN has been able to capture the influence of pressure and composition in combustion prediction. The CNN applies some extra delay for VGTs in comparison to the WG (Figure 5_D). Systematically, from 1500m in advance, p3 it is higher for the WG, this leads to a higher trapping ratio (Figure 5_E) and residuals fraction. Trapping ratio, is defined according to equation (2),

$$TR = \frac{\sum_{i=1}^{n-cylinder} m_{ub,nf,t}}{\sum_{i=1}^{n-cylinder} \oint \dot{m}_{ub,nf,iv}} \qquad (2)$$

where the upper term represents the unburned-gas (ub), non-fuel (nf), trapped (t) in cylinder "i" and the denominator represents the complete air mass flow through cylinder "i" intake valves (iv). In all, the presence of residuals enables the combustion advance due to the reduced oxygen fraction and higher specific heat. As a result, the best BSFC is found for the WG from 1500 to 3000 rpm. From 3000 in advance, it is mixture enrichment the main parameter that causes BSFC differences.

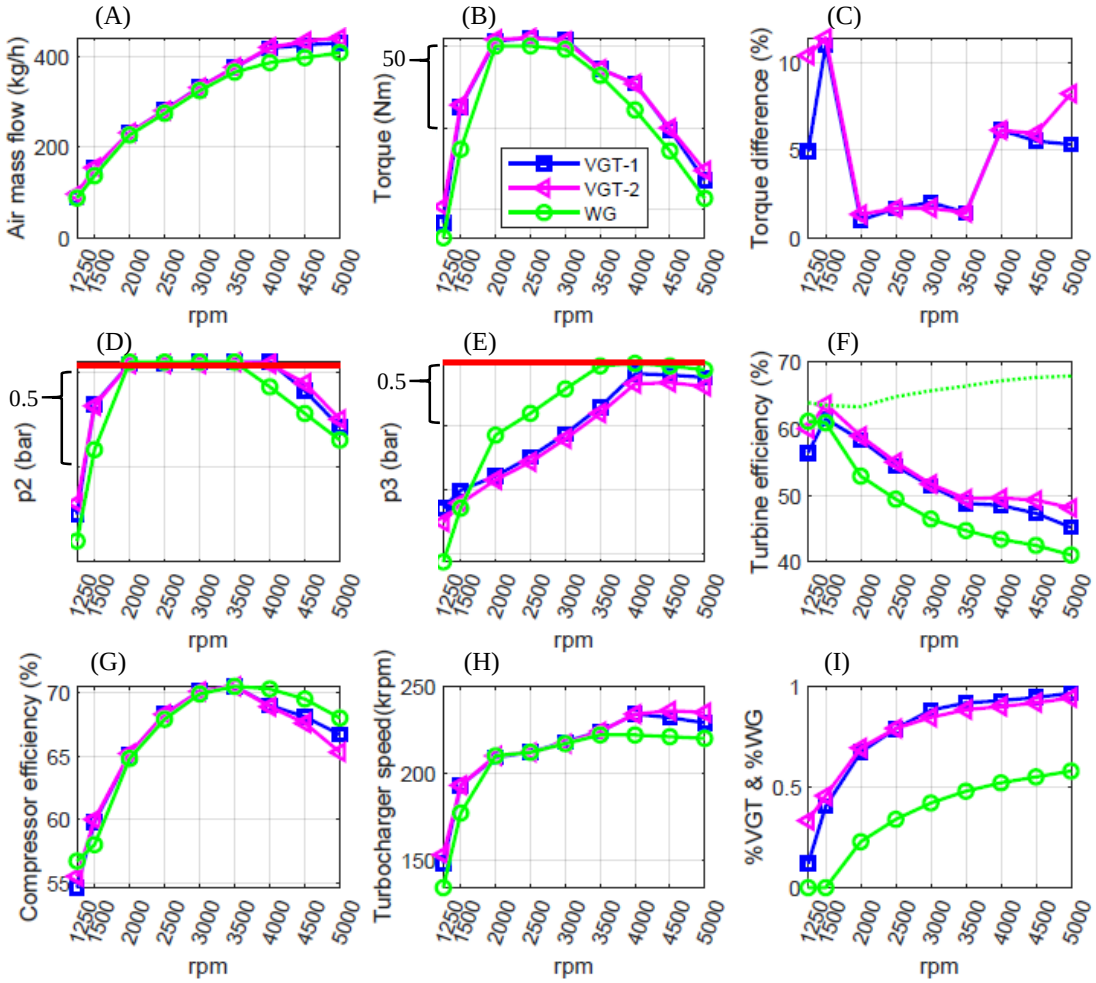

Figure 4: Performance analysis for full load results at sea level: VGT_1, VGT_2 and WG

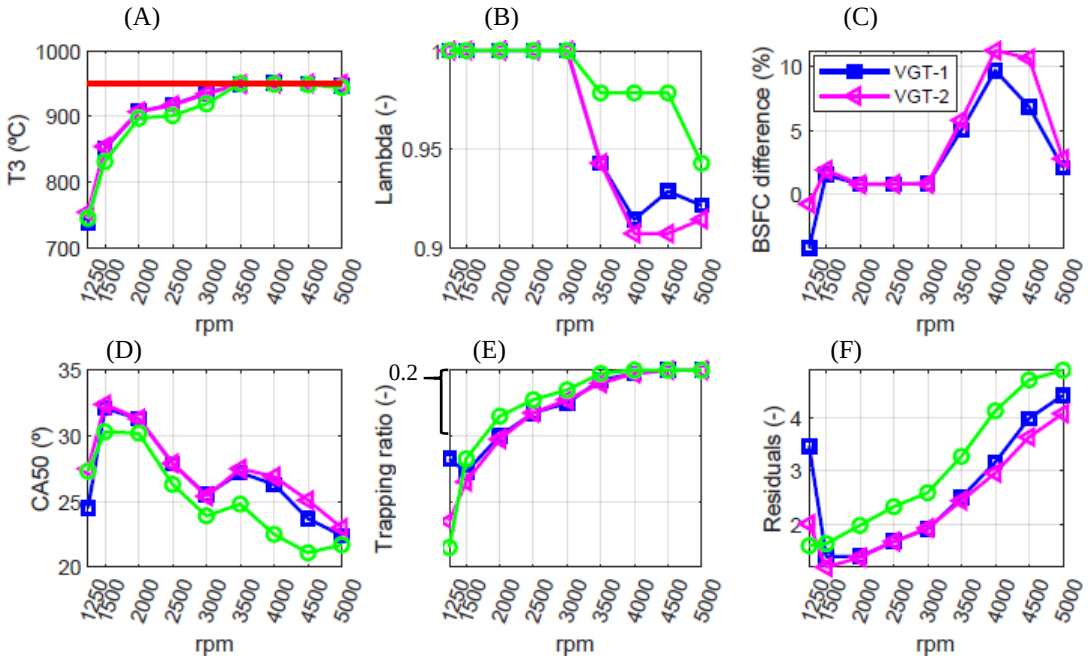

Figure 5: Efficiency and combustion results at sea level: VGT_1, VGT_2 and WG

If EGR is intended to be used all over the engine operative map (even in full loads), its usage could help for combustion phasing due to its potential to reduce knocking combustion [36]. This would help optimize engine BSFC together with the reduction of enrichment, as stated by Shen et al [37]. In that case, it would be of high interest to compensate the extra combustion delay for the VGT cases in comparison to the WG. As previously analyzed, the higher boost pressure enhances knock phenomena resulting in a more delayed combustion for the VGTs. This is even more noticeable in the low-end torque. Furthermore, if EGR was used in the complete engine range, higher boost pressure would be required to compensate the decrease in oxygen concentration and still ensure stoichiometric combustion. In this situation, VGT turbines may present a great advantage since the higher efficiency provides them with a wider operative margin.

3.2 Full load results in altitude (1300m)

It has been demonstrated that WG technology implies a limitation for engine complete performance at certain operating conditions. However, the authors have included a study under more adverse working conditions. Thus, full load curves have been simulated for WG and VGT_2 at 1300m of altitude (the homologating extended altitude for RDE). The main results are collected in Figure 6. Magenta continuous line, which corresponds to VGT_2 at sea level, is represented as a reference. Dotted lines correspond to the altitude cases. It is evidenced that air mass flow (Figure 6_A) and torque (Figure 6_B) suffer a dramatic decrease when comparing results at 1300m against sea level.

Figure 6_C shows how the effect of altitude has diminished the engine torque for the VGT_2 (dashed magenta series). This series is calculated according to equation (3). The torque deterioration goes from 2.5% to 14.5% approximately.

$$Altitude\ influence = \frac{VGT_{1300m} - VGT_{0m}}{VGT_{0m}} * 100 \quad (3)$$

The main reason for the air mass flow and torque decrease with respect to sea level is the boost pressure (Figure 6_D). The reason for the decay in the boost pressure depends on the speed range being analyzed. From 4500 to 5000 rpm for the VGT_2, the turbocharger speed implies a new constraint at 1300m (Figure 6_E). In the middle range (2000-4000), compressor outlet temperature (T2) is the main parameter that limits boost pressure in altitude conditions (Figure 6_F). This is due to the higher compressor pressure ratio requirement to target a given boost pressure. Similar T2 trend was found by Mansouri et al. [38] for a WG turbocharger, implying a deterioration also in the intake manifold temperature and volumetric efficiency if the charge air cooler cannot compensate the T2 increase. On the contrary, at sea level and in the range of 2000 to 4000 rpm, the maximum p2' was achieved without any other limitation (see Figure 6_D). In the low-end torque, for the VGT_2,

surge is the limiting parameter for both: sea level and 1300m. VGT position it is slightly further closed to damp the effect of the altitude. However surge limit gives as a result a lower boost pressure than the one at sea level.

The difference between VGT_2 and WG at altitude is also depicted in Figure 6_C (dotted black series), which is calculated by means of equation (4).

$$Tech.difference = \frac{VGT_{1300m} - WG_{1300m}}{WG_{1300m}} * 100 \quad (4)$$

Technology difference (at altitude) shows that VGT_2 improves the WG results by a 14-22% in the low-end torque, while from 2000rpm in advance a 2-5% improvement is predicted.

Torque differences between technologies in altitude are due to different reasons depending on the engine speed range:

- For the 2000-5000 rpm range higher engine torque is systematically predicted for VGT_2 at 1300m. The main reason for the torque difference is the higher air mass flow for the VGT, caused by the lower p3 (see Figure 6_H). This difference is due to a lower turbine efficiency in the WG series at 1300 m (see Figure 6_I).
- In the low-end torque, technology differences in altitude are directly attributed to boost pressure differences (see Figure 6_D). This is due to the improved matching of the VGT_2 over the engine mass-flow range: VGT compensates partially the effect of altitude by a slightly further closure, until compressor surge is reached. In the case of the WG, since the mechanism is fully closed even at sea level, there is no margin to damp the effect of altitude. The previous results in higher torque differences than the ones between technologies at sea level.

Finally, Figure 6_J shows how from 3500 in advance, mixture enrichment for the VGT is closer to stoichiometric in altitude than at sea level, while T3 is still properly controlled

(Figure 6_K). This is one of the main reasons why a 5-9.5% improvement in BSFC is shown in Figure 6_L for the VGT_2 (dashed magenta series) calculated according to equation (3). BSFC difference between technologies it is also shown in Figure 6_L, (dotted black series) calculated according to equation (4). The leaner mixture seen in the WG in comparison to the VGT in altitude operation explains the BSFC differences observed.

Figure 7_A represents the compressor map and the operative working points for both VGT_2 at sea level and at 1300m. Figure 7_B shows the same information for the WG turbine. The effect of altitude is mainly noticeable from 2000 rpm in advance leading the turbocharger to speed up. The last result goes in hand with T2 limitations in altitude conditions. When looking at the highlighted points in Figure 7_A, which correspond to 1250 and 1500 rpm, hardly noticeable differences are found between both series: surge limits the compressor operative point at sea level and in altitude, consequently the effect of altitude cannot be detected at the compressor map. However, as previously pointed out, the WG turbine cannot compensate the effect of altitude, preventing the turbocharger from speeding up to the desired value or until any limit is reached. This is evidenced in the compressor map, especially in 1500, where the boost pressure decreases as a consequence of turbocharger lower rpms.

3.3 Partial load results

The engine speed range in this study goes from 2000 to 4000 rpm. The simulation strategy was to target a given torque value corresponding to the area of the engine operation where the transition from throttled to boosted operation is performed. As it can be seen in Figure 8_A, no significant BSFC differences are observed. BSFC difference is calculated according to equation (5).

$$Tech.difference = \frac{VGT_{PL} - WG_{PL}}{WG_{PL}} * 100 \qquad (5)$$

The VGT technology implies higher restriction to the air mass flow circulation. As a result, higher p3 is reached (see Figure 8_B). Even though, there is no penalty in terms of BSFC or pumping losses (Figure 8_A and Figure 8_C). The reason is that even if p3 is around 0.04 bar higher for the VGT technology, the throttle body compensates the extra p3 with some extra p2' (see dotted series in Figure 8_E) for the requested torque.

The combustion neural network is sensitive to p2' and p3. This is why slight differences are observed in terms of CA50 (see Figure 8_F). Higher p3 values lead to more residuals in the combustion chamber. The presence of more residuals allows for a slight combustion advance.

In previous studies such as in the one from Kapoor et al [39], turbine maps were optimized for each engine operative area. They concluded that for the partial load working points the differences induced by turbine maps were almost negligible (hardly reaching values of 0.9 g/kWh). Similar results were obtained and concluded in this study, since BSFC differences reached a maximum value of 1.1g/kWh.

If by chance, after a stationary working point, a sudden load demand was requested, the VGT turbocharged engine response could be faster. It is evident that the turbocharger is far more accelerated (around 22 krpm systematically, whatever working point). In addition, the pressure in the routing between the throttle and the compressor is also higher. This means that after the sudden throttle opening a higher torque delivery may be expected, at least in the very early cycles, which are the most critical ones in the transient response of highly turbocharged engines.

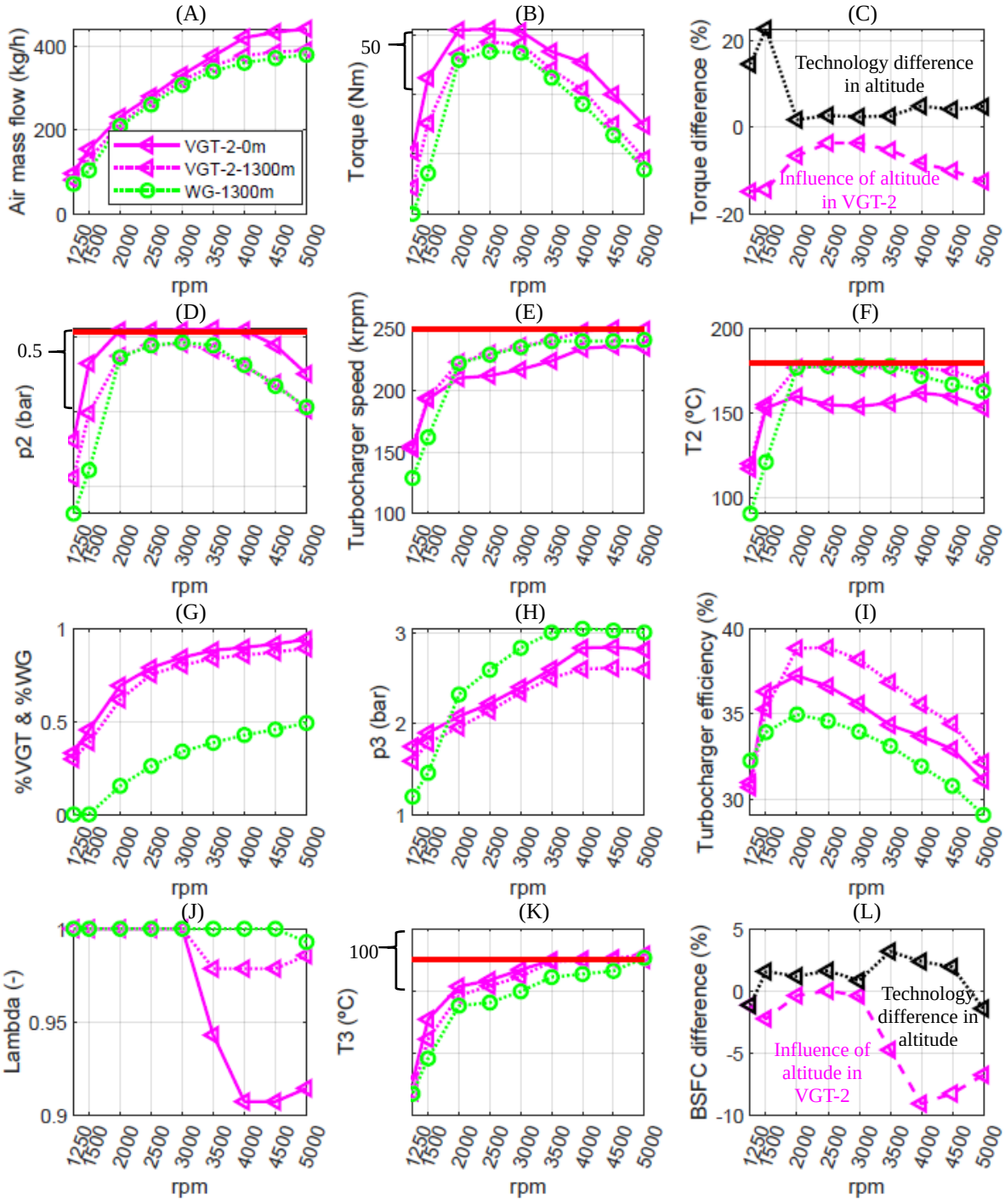

Figure 6: Altitude engine simulations with VGT-2-0m for reference

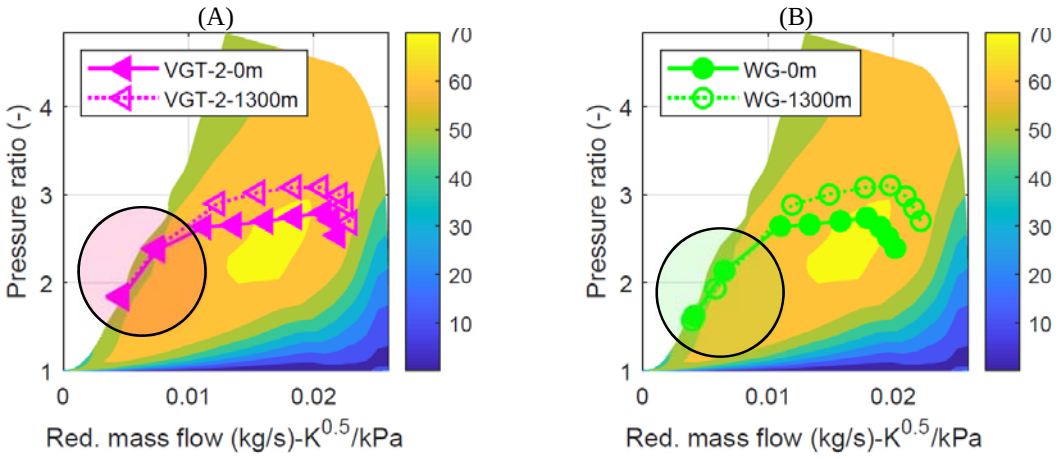

Figure 7: Compressor map and working points at altitude and at sea level: (A) for VGT_2 and (B) for WG. Low-end torque highlighted

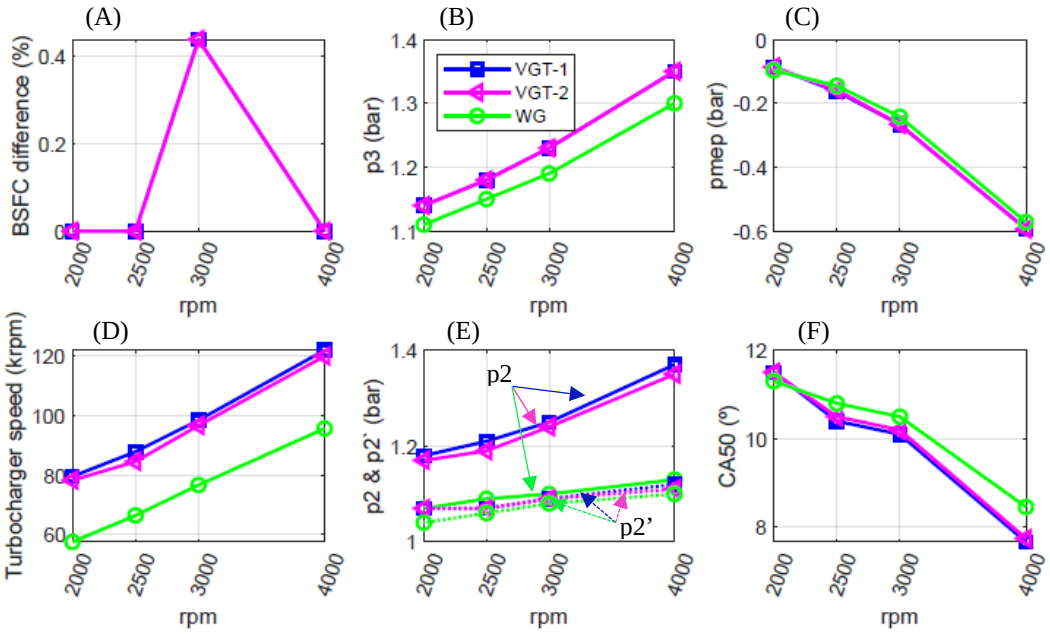

Figure 8: Partial load model results

4. Conclusions

In the current paper, a methodology to consistently analyze the impact of different turbine technologies for gasoline direct-injection engines is presented and applied to the comparison of waste-gate vs. variable geometry turbines. In a first step, experiments were performed on a multi-cylinder engine for one waste-gate and two variable geometry turbine samples. The experimental matrix covered both full-load and partial-load conditions. However, these results showed to be affected by differences in the compressor design, which was different for each sample, as well as unintended variations in the test boundary conditions (such as the ambient temperature and pressure). In order to compensate for these variabilities, a fully validated 1D engine model, including adiabatized turbocharger maps, is used. The model is adapted to include the same compressor map regardless the turbine. Then, this model is applied to evaluate the impact of VGT implementation in full-load performance, including sea level as well as an altitude of 1300 m, and part-load operation. Once the methodology is applied very similar trends are achieved for both VGT samples, which confirms the suitability of the methodology to provide a fair comparison between technologies.

Regarding the comparison between waste-gate and variable geometry turbine, the following conclusions can be drawn:

- At sea level, VGT technology provides advantages in both low-end torque (1250-1500 rpm) and high-speed operation (from 4000 rpm). At low speeds, this advantage comes from a higher boosting capability, moving the compressor operating point along the surge line. As the engine speed increases, the main driver becomes the turbine efficiency since the waste-gate is limited by maximum exhaust manifold pressure. However, this comes at the expense of higher fuel enrichment to maintain the temperature below the turbine inlet limitation resulting in higher fuel consumption.

- In altitude, the VGT provides further advantage also in the intermediate engine speed range, since the waste-gate operates already close to its maximum capability (fully close position), while the VGT shows some extra margin to compensate the higher compressor pressure ratio needed.
- At partial-load, VGT samples provide higher boosting pressure due to the higher enthalpy arriving to the turbine. This results in an enlargement of the throttled operation. However, the final impact on pumping losses and fuel consumption is limited thanks to the higher VGT efficiency.

ACKNOWLEDGEMENTS

Alejandro Gómez Vilanova is partially supported through contract: Ayuda de Formación de Profesorado Universitario (FPU18/04811). The authors wish to thank Vicente Esteve Ferrer for his invaluable work during the experimental campaign**.**

References

[1] Gross M, Sonnberger M. How the diesel engine became a “dirty” actant: Compression ignitions and actor networks of blame. Energy Res Soc Sci 2020;61:101359. doi:10.1016/j.erss.2019.101359.

[2] Abdul-Manan AFN, Won HW, Li Y, Sarathy SM, Xie X, Amer AA. Bridging the gap in a resource and climate-constrained world with advanced gasoline compression-ignition hybrids. Appl Energy 2020;267:114936. doi:10.1016/j.apenergy.2020.114936.

[3] Joshi A. Review of Vehicle Engine Efficiency and Emissions. SAE Tech Pap 2020;2020-April:1–29. doi:10.4271/2020-01-0352.

[4] Li Y, Zhao H, Stansfield P, Freeland P. Synergy between Boost and Valve Timings in a Highly Boosted Direct Injection Gasoline Engine Operating with Miller Cycle. SAE

Tech Pap 2015;2015-April. doi:10.4271/2015-01-1262.

[5] Miller J, Taylor J, Freeland P, Warth M, Dingelstadt R, Mueller R. Future gasoline engine technology and the effect on thermal management and real world fuel consumption. SAE Tech Pap 2013;2. doi:10.4271/2013-01-0271.

[6] Geng W, Lou D, Wang C, Zhang T. A cascaded energy management optimization method of multimode power-split hybrid electric vehicles. Energy 2020;199:117224. doi:10.1016/j.energy.2020.117224.

[7] García A, Monsalve-Serrano J, Martínez-Boggio S, Wittek K. Potential of hybrid powertrains in a variable compression ratio downsized turbocharged VVA Spark Ignition engine. Energy 2020;195:117039. doi:10.1016/j.energy.2020.117039.

[8] Tagliaferri C, Evangelisti S, Acconcia F, Domenech T, Ekins P, Barletta D, et al. Life cycle assessment of future electric and hybrid vehicles: A cradle-to-grave systems engineering approach. Chem Eng Res Des 2016;112:298–309. doi:10.1016/j.cherd.2016.07.003.

[9] Serrano JR, Novella R, Piqueras P. Why the development of internal combustion engines is still necessary to fight against global climate change from the perspective of transportation. Appl Sci 2019;9. doi:10.3390/app9214597.

[10] Mehta S, Hemamalini S. A Dual Control Regenerative Braking Strategy for Two-Wheeler Application. Energy Procedia 2017;117:299–305. doi:10.1016/j.egypro.2017.05.135.

[11] Lang O, Geiger J, Habermann K, Wittler M. Boosting and direct injection -synergies for future gasoline engines. SAE Tech Pap 2005;2005. doi:10.4271/2005-01-1144.

[12] Qian Y, Gong Z, Shao X, Tao C, Zhuang Y. Numerical study of the effect of combustion chamber structure on scavenging process in a boosted GDI engine. Energy 2019;168:9–29. doi:10.1016/j.energy.2018.11.080.

[13] Zhu D, Zheng X. Asymmetric twin-scroll turbocharging in diesel engines for energy

and emission improvement. Energy 2017;141:702–14. doi:10.1016/j.energy.2017.07.173.

[14] Mingyang Y, botas Ricardo M, Kangyao D, Yangjun Z, Xinqian Z. Unsteady influence of Self Recirculation Casing Treatment (SRCT) on high pressure ratio centrifugal compressor. Int J Heat Fluid Flow 2016;58:19–29. doi:10.1016/j.ijheatfluidflow.2015.12.004.

[15] Rajoo S, Romagnoli A, Martinez-Botas RF. Unsteady performance analysis of a twin-entry variable geometry turbocharger turbine. Energy 2012;38:176–89. doi:10.1016/j.energy.2011.12.017.

[16] Serrano JR, Navarro R, García-Cuevas LM, Inhestern LB. Turbocharger turbine rotor tip leakage loss and mass flow model valid up to extreme off-design conditions with high blade to jet speed ratio. Energy 2018;147:1299–310. doi:10.1016/j.energy.2018.01.083.

[17] Serrano JR, Arnau FJ, García-Cuevas LM, Inhestern LB. An innovative losses model for efficiency map fitting of vaneless and variable vaned radial turbines extrapolating towards extreme off-design conditions. Energy 2019;180:626–39. doi:10.1016/j.energy.2019.05.062.

[18] Ding Z, Zhuge W, Zhang Y, Chen H, Martinez-Botas R, Yang M. A one-dimensional unsteady performance model for turbocharger turbines. Energy 2017;132:341–55. doi:https://doi.org/10.1016/j.energy.2017.04.154.

[19] Bozza F, De Bellis V, Teodosio L. Potentials of cooled EGR and water injection for knock resistance and fuel consumption improvements of gasoline engines. Appl Energy 2016;169:112–25. doi:10.1016/j.apenergy.2016.01.129.

[20] Sandoval OR, Fonda MV, Roso VR, da Costa RBR, Valle RM, Baêta JGC. Computational technique for turbocharger transient characterization using real driving conditions data. Energy 2019;186:115822.

doi:https://doi.org/10.1016/j.energy.2019.07.152.

[21] Feneley AJ, Pesiridis A, Andwari AM. Variable Geometry Turbocharger Technologies for Exhaust Energy Recovery and Boosting-A Review. Renew Sustain Energy Rev 2017;71:959–75. doi:10.1016/j.rser.2016.12.125.

[22] Sjerić M, Taritaš I, Tomić R, Blažić M, Kozarac D, Lulić Z. Efficiency improvement of a spark-ignition engine at full load conditions using exhaust gas recirculation and variable geometry turbocharger – Numerical study. Energy Convers Manag 2016;125:26–39. doi:10.1016/j.enconman.2016.02.047.

[23] Andersen J, Karlsson E, Gawell A. Variable turbine geometry on SI engines. SAE Tech Pap 2006;2006:776–90. doi:10.4271/2006-01-0020.

[24] Shimizu K, Sato W, Enomoto H, Yashiro M. Torque control of a small gasoline engine with a variable nozzle turbine turbocharger. SAE Tech Pap 2009:1–7.

[25] Noga M. Application of VNT turbocharger in spark ignition engine with additional expansion of exhaust gases. Teh Vjesn 2018;25:1575–80. doi:10.17559/TV-20160211230747.

[26] Tang H, Copeland C, Akehurst S, Brace C, Davies P, Pohorelsky L, et al. A novel predictive semi-physical feed-forward turbocharging system transient control strategy based on mean-value turbocharger model. Int J Engine Res 2017;18:765–75. doi:10.1177/1468087416670052.

[27] Ericsson G, Angstrom HE, Westin F. Optimizing the transient of an SI-engine equipped with variable cam timing and variable turbine. SAE Tech Pap 2010;3:903–15. doi:10.4271/2010-01-1233.

[28] Wang Y, Conway G, McDonald J, Birckett A. Predictive GT-power simulation for VNT matching to EIVC strategy on a 1.6 L turbocharged gdi engine. SAE Tech Pap 2019;2019-April:1–12. doi:10.4271/2019-01-0192.

[29] Serrano JR, Arnau FJ, De La Morena J, Gómez-vilanova A, Guilain S, Batard S. A

methodology to calibrate gas-dynamic models of turbocharged petrol engines with variable geometry turbines and with focus on dynamics prediction during tip-in load transient tests. Proc ASME Turbo Expo 2020;2020-june:22–6.

[30] Serrano JR, Arnau FJ, García-Cuevas LM, Gómez-Vilanova A, Guilain S, Batard S. A Methodology for Measuring Turbocharger Adiabatic Maps in a Gas-Stand and its Usage for Calibrating Control Oriented and 1D Models at Early ICE Design Stages 2019. doi:10.1115/ICEF2019-7125.

[31] Pla B, De la Morena J, Bares P, Jiménez I. Cycle-to-cycle combustion variability modelling in spark ignited engines for control purposes. Int J Engine Res 2019. doi:10.1177/1468087419885754.

[32] Choi S, Kolodziej CP, Hoth A, Wallner T. Development and Validation of a Three Pressure Analysis (TPA) GT-Power Model of the CFR F1/F2 Engine for Estimating Cylinder Conditions. SAE Tech Pap 2018;2018-April:1–9. doi:10.4271/2018-01-0848.

[33] Galindo J, Luján JM, Serrano JR, Hernández L. Combustion simulation of turbocharger HSDI Diesel engines during transient operation using neural networks. Appl Therm Eng 2005;25:877–98. doi:10.1016/j.applthermaleng.2004.08.004.

[34] Serrano J, Climent H, Navarro R, González-Domínguez D. Methodology to Standardize and Improve the Calibration Process of a 1D Model of a GTDI Engine. SAE Tech Pap 2020;2020-April:1–13. doi:10.4271/2020-01-1008.

[35] Tang H, Pennycott A, Akehurst S, Brace CJ. A review of the application of variable geometry turbines to the downsized gasoline engine. Int J Engine Res 2015;16:810–25. doi:10.1177/1468087414552289.

[36] Franken T, Mauss F, Seidel L, Gern MS, Kauf M, Matrisciano A, et al. Gasoline engine performance simulation of water injection and low-pressure exhaust gas recirculation using tabulated chemistry. Int J Engine Res 2020;(in press). doi:10.1177/1468087420933124.

[37] Shen X, Shen K, Zhang Z. Experimental study on the effect of high-pressure and low-pressure exhaust gas recirculation on gasoline engine and turbocharger. Adv Mech Eng 2018;10:1–8. doi:10.1177/1687814018809607.

[38] Mansouri H, Ommi F. Performance prediction of aircraft gasoline turbocharged engine at high-altitudes. Appl Therm Eng 2019;156:587–96. doi:10.1016/j.applthermaleng.2019.04.116.

[39] Kapoor P, Costall AW, Sakellaridis N, Hooijer J, Lammers R, Tartoussi H, et al. Adaptive Turbo Matching: Radial Turbine Design Optimization through 1D Engine Simulations with Meanline Model in-the-Loop. SAE Tech Pap 2018;2018-April:1–15. doi:10.4271/2018-01-0974.